

A molecular superfluid: non-classical rotations in doped para-hydrogen clusters

Hui Li,^{1,2} Robert J. Le Roy,¹ Pierre-Nicholas Roy,^{1,*} and A.R.W. McKellar^{3,†}

¹ *Department of Chemistry, University of Waterloo,
Waterloo, Ontario N2L 3G1, Canada*

² *Institute of Theoretical Chemistry,
State Key Laboratory of Theoretical and Computational Chemistry,
Jilin University, 2519 Jiefang Road,
Changchun 130023, People's Republic of China*

³ *Steacie Institute for Molecular Sciences,
National Research Council of Canada,
Ottawa, Ontario K1A 0R6, Canada*

**pnroy@uwaterloo.ca*

†Robert.McKellar@nrc-cnrc.gc.ca

(Dated: May 30, 2022; Published as: Phys. Rev. Lett. **105**, 133401 (2010))

Clusters of para-hydrogen ($p\text{H}_2$) have been predicted to exhibit superfluid behavior, but direct observation of this phenomenon has been elusive. Combining experiments and theoretical simulations, we have determined the size evolution of the superfluid response of $p\text{H}_2$ clusters doped with carbon dioxide (CO_2). Reduction of the effective inertia is observed when the dopant is surrounded by the $p\text{H}_2$ solvent. This marks the onset of molecular superfluidity in $p\text{H}_2$. The fractional occupation of solvation rings around CO_2 correlates with enhanced superfluid response for certain cluster sizes.

PACS numbers: 36.40.-c, 36.40.Ei, 36.40.Mr, 67.25.dw

Superfluidity has been well characterized in the bulk liquid phase [1]. In a breakthrough experiment, Grebenev, Toennies, and Vilesov observed superfluidity in helium nanodroplets [2], introducing a new way of investigating finite quantum systems [3]. Only atomic helium has been known to exhibit this behaviour at liquid-like densities, and the direct observation of superfluidity in a molecular system has remained elusive. The most likely candidate for a molecular superfluid is para-hydrogen ($p\text{H}_2$), because of its bosonic character, low mass, and weak intermolecular forces. In order to confirm superfluidity in molecular hydrogen, an experimental determination of the so-called superfluid response or non-classical rotational inertia [1] is required.

The spectroscopic observation of nearly free molecular rotation in helium nanodroplets [2, 3] has motivated several studies aimed at providing an understanding of superfluidity at the nanoscale in finite systems. Rovibrational spectra of linear molecules such as OCS in helium droplets are characterized by narrow lines indicative of coherent rotation and decoupling from the solvent [2]. Most importantly, the spectroscopic rotational constant B [4] of the molecular dopant is renormalized by the helium environment. B is inversely proportional to the effective moment of inertia of the system, so in a normal classical system, the inertia should grow monotonically with system size N . A key experiment on OCS-doped clusters with a few ($N = 1 - 8$) helium atoms has shown that their effective inertia could actually be greater than that of larger droplets [5]. Thus a decoupling mechanism must exist in order to stop the growth of the effective inertia as the cluster grows beyond $N = 8$. The turnaround marks the onset of superfluidity [5].

Theoretical analysis has later shown that the size evo-

lution of B was related to that of the superfluid fraction, defined as the deviation from a classical response to rotation [6–8]. B constants were also used to estimate the ‘experimental’ superfluid fraction [7, 8]. Theorists have predicted superfluidity in $p\text{H}_2$ clusters [9], but the direct observation of superfluid response in doped $p\text{H}_2$ clusters has remained elusive. Simulation work predicted superfluidity for OCS-doped $p\text{H}_2$ clusters [10, 11] with a turnaround of B at $N = 14$. However, this prediction is not yet confirmed by experiment, since published measurements only extend to $N = 7$ [12]. In other experiments, superfluidity was inferred for doped $p\text{H}_2$ clusters embedded in helium nanodroplets based on the behavior of the Q branch of the rovibrational spectrum [13–16]. Moore and Miller performed related experiments on doped HD clusters [17–19]. These results motivated our search for a system where the superfluidity of $p\text{H}_2$ could be discerned.

Here we report confirmation of molecular superfluid behavior in doped $p\text{H}_2$ clusters, based on spectroscopic determination of their non-classical rotational inertia probed by CO_2 . Our main result confirms earlier theoretical predictions that $p\text{H}_2$ clusters could become superfluid [9], and lends weight to experiments that have shown evidence of superfluidity in doped $p\text{H}_2$ clusters embedded in helium nanodroplets [13–16]. We have measured infrared spectra and performed finite-temperature path-integral Monte Carlo (PIMC) simulations to support our findings.

The experimental apparatus has been described elsewhere [20]. Backing pressures in the range of 5 to 25 atmospheres were used, and the jet nozzle was cooled (-20 to 100 °C). Effective cluster rotational temperatures were 0.3 to 1 K. Since the measurements were performed for

$^{13}\text{C}^{16}\text{O}_2$ and $^{13}\text{C}^{18}\text{O}_2$, the vibrational frequency shifts and B rotational parameters reported here were scaled to values appropriate to $^{12}\text{C}^{16}\text{O}_2$ for comparison with theory. Due to CO_2 nuclear spin statistics and the low temperature of the jet expansion, only three transitions are generally observed for each cluster: $R(0)$, $R(2)$, and $P(2)$. We fit these lines in terms of three parameters: band origin, B rotational constant, D centrifugal distortion constant.

Details of the PIMC calculation method are described elsewhere [7, 21–23]. It relies on the so-called worm algorithm [24, 25] to account for bosonic exchange. We used a recent $\text{H}_2\text{-H}_2$ interaction potential [26] along with our own $\text{H}_2\text{-CO}_2$ potential energy surfaces [27]. The calculations were performed for a low temperature (0.5 K), with 256 translational and 128 rotational time slices. A total number of $10^7\text{-}10^8$ Monte Carlo steps for each simulation yielded satisfactory error bars. Figure 1a is a mon-

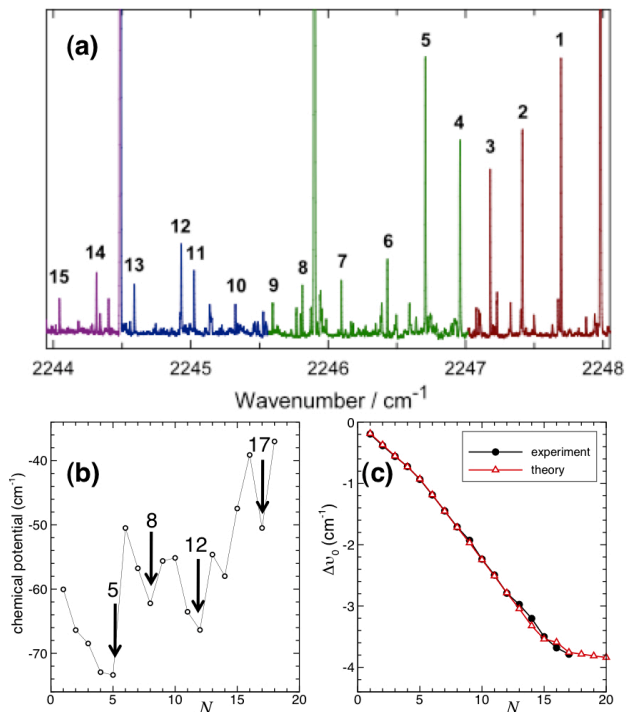


FIG. 1. (color online) (a) Observed spectrum with assigned $R(0)$ transitions labeled by cluster size, N . The three strongest (off-scale) transitions are the $P(4)$, $P(2)$, and $R(0)$ transitions of the CO_2 monomer. (b) Calculated chemical potential (in wavenumbers; $1.0 \text{ cm}^{-1} = 1.438769 \text{ K}$) versus N . (c) Measured (filled circles) and theoretical (open triangles) shifts of the CO_2 asymmetric stretch vibrational frequency versus N .

tage of 4 traces where the experimental conditions were

optimized for each cluster size range. For this reason, and because laser power varies, relative line intensities are not quantitative. However, their qualitative trend is real, reflecting the behavior of the chemical potential (the energy difference between adjacent cluster sizes) curve in Fig. 1b, with $N = 5$ and 12 being relatively stable (larger negative chemical potential) and $N = 6, 9$ and 10 less so. Line assignments for $N < 8$ are straightforward, and confirm the accuracy of the theoretical vibrational shifts. For $N \geq 8$ the line assignments are not so obvious. However, by using the theoretical CO_2 vibrational shifts in Fig. 1(c) to help guide the assignments, a convincing scheme is achieved which is more complete and self-consistent than any other. The special nature of $N = 12$ is directly evident without any reference to theory: its transitions are noticeably stronger, indicating a local maximum in the cluster population, which is consistent with the local maximum in the absolute value of the chemical potential in Fig. 1(b).

Magic numbers indicative of particularly stable structures are observed for $N = 5, 8, 12, 14$, and 17. In Fig. 1(c), the subtle change in slope at $N = 5$ is associated with filling of a ‘donut ring’ of 5 $p\text{H}_2$ molecules around the CO_2 axis. For $5 < N < 9$ the additional $p\text{H}_2$ start populating a second ring. The excellent agreement between the theoretical and experimental vibrational shifts attests to the quality of the interaction potentials used in the simulations.

The structural evolution is shown in Fig. 2 by the patterns of the $p\text{H}_2$ density contours in the frame of the CO_2 molecule. Occupation numbers of ‘donut rings’ and ‘terminal caps’ are indicated. The occupation numbers, which add up to N , were obtained by integrating the $p\text{H}_2$ density in each ring and rounding to the nearest simple fraction. The boundary region between two rings was set as the minimum in the density. A central ‘donut ring’ is filled for $N = 5$ and a full solvation shell is observed for $N = 17$; the latter cluster size marks a more pronounced change in slope in the vibrational shift curve of Fig. 1c. The filling of a second centred ring starts at $N = 18$.

Figure 3a shows the effective B constant, B_{eff} as a function N . Calculations based on a dipole-dipole correlation function can be compared directly to experiment. In earlier work on helium clusters doped with CO_2 [22], N_2O [7, 21], and HCCCN [8], the calculated B was in very good agreement with experiment. The present theoretical values agree remarkably well with experiment, and capture the overall behavior of the size evolution of $B_{\text{eff}}^{\text{exp}}$. However, some deviations are observed for $N \geq 13$. These discrepancies may be attributed to the finite (non-zero) temperature of the simulations.

A key question is whether or not $B_{\text{eff}}^{\text{exp}}$ really probes superfluidity. For systems undergoing rotation, the superfluid fraction is defined in terms of the non-classical rotational inertia using a two-fluid model [28, 29] which assumes that the total density of the fluid is the sum of

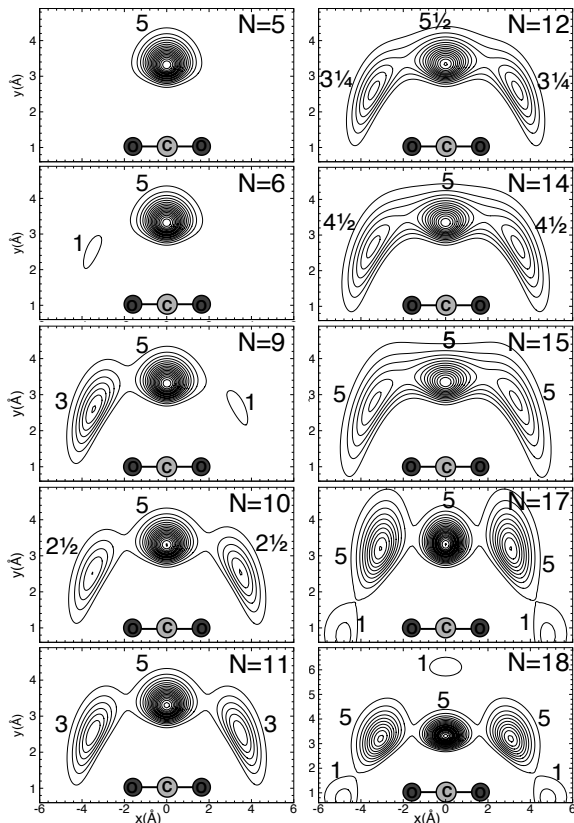


FIG. 2. Contours of two dimensional projections of the $p\text{H}_2$ density in the CO_2 frame for representative N values. Whole and fractional occupation numbers are shown.

contributions from normal and superfluid components: $\rho = \rho_s + \rho_n$. The superfluid fraction is $f_s = \frac{\rho_s}{\rho}$ while the normal fraction is $f_n = \frac{\rho_n}{\rho}$, defined as $f_n = \frac{I_{\text{eff}}}{I_{\text{cl}}}$, the ratio of the effective (I_{eff}) over the classical (I_{cl}) inertia of $p\text{H}_2$. The calculated f_s shown in Fig.3b corresponds to the perpendicular response with respect to the CO_2 axis. The experimental f_s was obtained using the approach proposed in Ref. [7], according to which $B_{\text{eff}}^{\text{exp}}$ defines the total moment of inertia of the system via the relation $B^{\text{exp}} = \frac{\hbar^2}{2I_{\text{total}}^{\text{exp}}}$. The effective inertia of $p\text{H}_2$ is obtained by subtracting the moment of inertia of CO_2 , $I_{\text{eff}}^{\text{exp}} = I_{\text{total}}^{\text{exp}} - I_{\text{CO}_2}$. An experimental estimate of f_s is presented in Fig. 3b. The experimental and theoretical f_s values agree fairly well in their overall behavior over a large range of sizes.

We conclude that within linear response theory, CO_2 can be used as a probe of f_s in $p\text{H}_2$ clusters. It is also possible to use the computed f_s to obtain two-fluid B constants. Such two-fluid values are presented in Fig. 3a. Their behavior is very close to that of $B_{\text{eff}}^{\text{exp}}$, and further confirms that CO_2 is a probe of superfluid response. To highlight the non-classical behaviour of I_{eff} ,

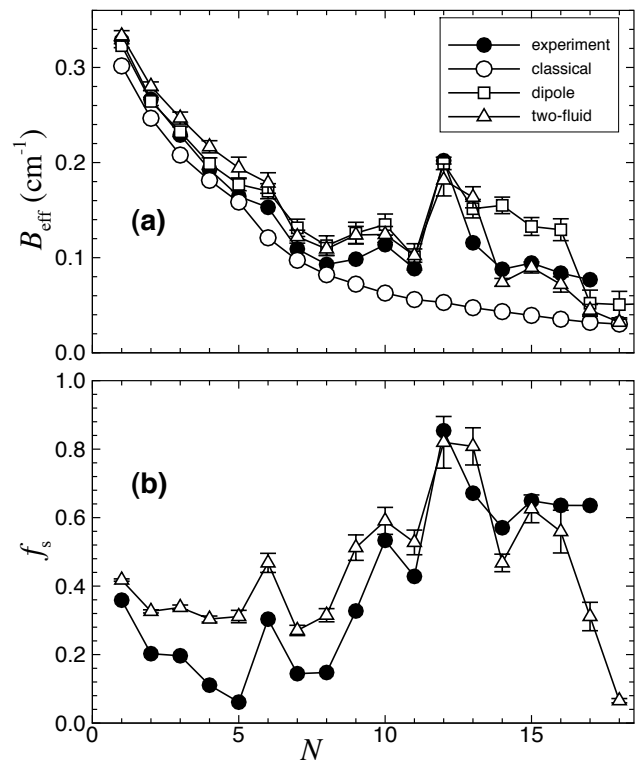


FIG. 3. (a) B_{eff} versus N from experiment (filled circles), and dipole-dipole (open squares), two-fluid (open triangles), and classical (open circles) calculations. (b) Experimental (filled circles) and calculated (open triangles) f_s versus N .

the effective B constants based on classical cluster inertia ($B_{\text{cl}} = \frac{\hbar^2}{2(I_{\text{cl}} + I_{\text{CO}_2})}$) are also shown in Fig. 3a. As expected, B_{cl} decreases monotonically with N .

Figure 4 shows the low and high $p\text{H}_2$ density regions in 3D for two cluster sizes [30]. For $N = 12$, the maximum in f_s , the low-density surface is continuous, except at the ends of the CO_2 axis. This is consistent with the enhanced bosonic exchanges associated with its larger f_s . For $N = 17$, the low-density ring regions are disconnected from one another, consistent with a lower f_s . For $N = 12$, the high-density surface is still highly delocalized within each ring, although the rings are no longer connected. For $N = 17$, pronounced localization is observed at high density, and one can clearly enumerate the individual $p\text{H}_2$ molecules. The orthographic top view for $N = 12$ (Fig. 4b) shows that the central ring is swollen to accommodate an additional fraction of a particle, while a similar view for $N = 17$ (Fig. 4e) shows that all three rings have similar radii with staggered particle placement.

Using CO_2 to probe superfluidity for doped $p\text{H}_2$ clusters in the $N = 1 - 18$ range, we provide the first direct measurement of f_s in a molecular system. A maximum in f_s is observed at $N = 12$. This value is confirmed by consistent experimental and theoretical results, and

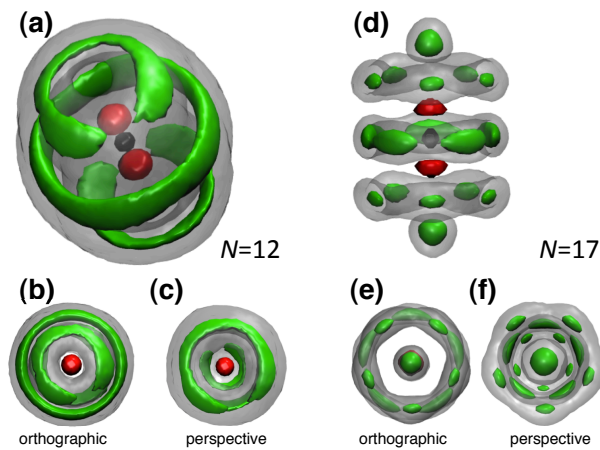


FIG. 4. (color online) Three-dimensional $p\text{H}_2$ densities [30]. (a) Side view for $N = 12$. (b) Top orthographic (or flat) view for $N = 12$. (c) Perspective view for $N = 12$. (d) side view for $N = 17$. (e) Top orthographic view for $N = 17$. (f) Perspective view for $N = 17$. The green (dark) and grey (light) colors respectively represent high and low densities.

is associated with the appearance of fractional ring occupation. Beyond this size, f_s decreases due to enhanced localization. There is a fine balance between the forces that cause localization, and bosonic exchanges that favour superfluidity. Localization dominates at higher N . A full solvation shell with pronounced localization is observed at $N = 17$; the computed f_s there is substantially lower than the experimental value. A possible explanation for this discrepancy is the finite (non-zero) temperature character of the PIMC simulation and the fact this f_s estimate is based on linear response theory. A lower temperature simulation could lead to a higher f_s due to quantum melting [31–33]. Whether or not larger clusters will be superfluid remains an open question. The localization modulated superfluid response may be viewed as the nanoscale analogue of the insulating to superfluid transitions observed in cold gases [34].

We acknowledge N. Blinov, M. Gingras, W. Jäger, F. McCourt, R. Melko, M. Nooijen, and P. Raston for discussions, the Natural Sciences and Engineering Research Council of Canada and the National Research Council of Canada for support, and the Shared Hierarchical Academic Research Computing Network for computing time.

[1] A. J. Leggett, *Rev. Mod. Phys.* **71**, S318 (1999).
 [2] S. Grebenev, J. P. Toennies, and A. F. Vilesov, *Science* **279**, 2083 (1998).
 [3] J. P. Toennies and A. F. Vilesov, *Angew. Chem.-Int. Edit.* **43**, 2622 (2004).
 [4] Half the energy spacing between the ground and first

excited rotational level.

[5] J. Tang, Y. J. Xu, A. R. W. McKellar, and W. Jäger, *Science* **297**, 2030 (2002).
 [6] F. Paesani, Y. Kwon, and K. B. Whaley, *Phys. Rev. Lett.* **94**, 153401 (2005).
 [7] Y. J. Xu, N. Blinov, W. Jäger, and P.-N. Roy, *J. Chem. Phys.* **124**, 081101 (2006).
 [8] W. Topic, W. Jäger, N. Blinov, P.-N. Roy, M. Botti, and S. Moroni, *J. Chem. Phys.* **125**, 144310 (2006).
 [9] P. Sindzingre, D. M. Ceperley, and M. L. Klein, *Phys. Rev. Lett.* **67**, 1871 (1991).
 [10] Y. Kwon and K. B. Whaley, *Phys. Rev. Lett.* **89**, 273401 (2002).
 [11] F. Paesani, R. E. Zillich, Y. Kwon, and K. B. Whaley, *J. Chem. Phys.* **122**, 181106 (2005).
 [12] J. M. Michaud and W. Jäger, *J. Chem. Phys.* **129**, 144311 (2008).
 [13] S. Grebenev, B. Sartakov, J. P. Toennies, and A. F. Vilesov, *Science* **289**, 1532 (2000).
 [14] S. Grebenev, B. Sartakov, J. P. Toennies, and A. Vilesov, *Phys. Rev. Lett.* **89**, 225301 (2002).
 [15] S. Grebenev, B. G. Sartakov, J. P. Toennies, and A. F. Vilesov, *Epl-Europhys Lett* **83**, 66008 (2008).
 [16] S. Grebenev, B. G. Sartakov, J. P. Toennies, and A. F. Vilesov, *J. Chem. Phys.* **132**, 064501 (2010).
 [17] D. T. Moore and R. E. Miller, *J. Chem. Phys.* **119**, 4713 (2003).
 [18] D. T. Moore and R. E. Miller, *J. Phys. Chem. A* **107**, 10805 (2003).
 [19] D. T. Moore and R. E. Miller, *J. Phys. Chem. A* **108**, 1930 (2004).
 [20] M. D. Brookes, C. H. Xia, J. Tang, J. A. Anstey, B. G. Fulsom, K. X. A. Yong, J. M. King, and A. R. W. McKellar, *Spectrochim. Acta A* **60**, 3235 (2004).
 [21] S. Moroni, N. Blinov, and P.-N. Roy, *J. Chem. Phys.* **121**, 3577 (2004).
 [22] N. Blinov and P.-N. Roy, *J. Low. Temp. Phys.* **140**, 253 (2005).
 [23] H. Li, N. Blinov, P.-N. Roy, and R. J. Le Roy, *J. Chem. Phys.* **130**, 144305 (2009).
 [24] M. Boninsegni, N. V. Prokof'ev, and B. V. Svistunov, *Phys. Rev. Lett.* **96**, 070601 (2006).
 [25] M. Boninsegni, N. V. Prokof'ev, and B. V. Svistunov, *Phys. Rev. E* **74**, 036701 (2006).
 [26] K. Patkowski, W. Cencek, P. Jankowski, K. Szalewicz, J. B. Mehl, G. Garberoglio, and A. H. Harvey, *J. Chem. Phys.* **129**, 094304 (2008).
 [27] H. Li, P.-N. Roy, and R. J. Le Roy, *J. Chem. Phys.* **132**, 214309 (2010).
 [28] D. M. Ceperley, *Rev. Mod. Phys.* **67**, 279 (1995).
 [29] E. W. Draeger and D. M. Ceperley, *Phys. Rev. Lett.* **90**, 065301 (2003).
 [30] The densities were calculated in a body-fixed frame determined from the instantaneous moment of inertia tensor of the whole cluster at each Monte Carlo step.
 [31] F. Mezzacapo and M. Boninsegni, *Phys. Rev. Lett.* **97**, 045301 (2006).
 [32] F. Mezzacapo and M. Boninsegni, *Phys. Rev. A* **75**, 033201 (2007).
 [33] J. E. Cuervo and P.-N. Roy, *J. Chem. Phys.* **128** (2008).
 [34] M. Greiner, O. Mandel, T. Esslinger, T. W. Hansch, and I. Bloch, *Nature* **415**, 39 (2002).